Supporting information for

Using heterostructural alloying to tune the structure and properties of the thermoelectric $Sn_{1-x}Ca_xSe$

Bethany E. Matthews[1], Aaron M. Holder[2], Laura T. Schelhas[3], Sebastian Siol[4†], James W. May[1], Michael R. Forkner[1], Derek Vigil-Fowler[4], Michael F. Toney[3,6], John D. Perkins[4], Brian P. Gorman[5], Andriy Zakutayev[4], Stephan Lany[4], Janet Tate[1].

[1]Department of Physics, Oregon State University, Corvallis, Oregon 97331, USA

[2]Department of Chemical and Biological Engineering, University of Colorado, Boulder, Colorado 80309, USA

[3]Applied Energy Programs, SLAC National Accelerator Laboratory, Menlo Park, CA 94025, USA

[4]National Renewable Energy Laboratory, Golden, CO 80401, USA

[5]Department of Metallurgical and Materials Engineering, Colorado School of Mines, Golden, CO 80401, USA

[6]Stanford Synchrotron Radiation Lightsource, SLAC National Accelerator Laboratory, Menlo Park, CA 94025, USA

†Present address: Empa, Swiss Federal Laboratories for Materials Science and Technology, Überlandstrasse 129, 8600 Dübendorf, Switzerland

Film Stoichiometry:

The $Sn_{1-x}Ca_xSe$ film stoichiometry, and in particular the Sn:Ca ratio in $Sn_{1-x}Ca_xSe$, is nominally controlled by the relative number of pulses directed at each target. To establish that the pulse count accurately reflects the actual film stoichiometry, several films, deposited between 220˚C and 320˚C, have been analyzed by wavelength-dispersive electron probe microanalysis (EPMA) in a CAMECA SX100 system. The EPMA beam size is about 10 μm and the composition resolution is approximately 0.1 atomic %. Fig. S1 shows that the cation stoichiometry on the 10-μm length scale in the $Sn_{1-x}Ca_xSe$ films is consistent with that expected from the pulse ratio at all deposition temperatures. We find very slightly more Ca in the film than expected from the pulse ratio, suggesting that CaSe has a higher sticking coefficient or is less likely to be scattered out of the plume than SnSe. The deviation $\Delta x \approx 0.03$ is too small to be of concern for this study, and all x values quoted in this paper are derived from the pulse count. EPMA also shows that the films are on average stoichiometric with a Se/(Sn+Ca+Se) ratio of 0.50 ± 0.03 for unoxidized films. The oxygen concentration in the films is at the limit of detection by EPMA. Occasionally, a film might exhibit an anomalously high oxygen concentration of about 40 atomic %. We exclude such films from this analysis.

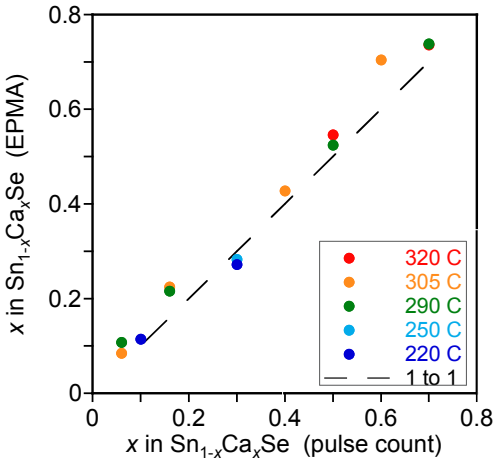

Fig. S1. Ca fraction x determined from EPMA and from PLD pulse count. The colors indicate the substrate deposition temperature.

The films are also characterized on the nanometer scale by x-ray energy dispersive spectroscopy (EDS) as discussed in the text. The stoichiometry measured by both methods gives the same results within the limitations of the measuring systems.

Film texture:

SnSe films grown at 370, 440, and 500° C are measured in the θ-2θ configuration to investigate the effect of substrate deposition temperature on texture. Fig. S2 shows that the (00ℓ) orientation is strong and increases at the higher temperatures, greatly enhancing the (002) and (006) reflections which are normally very weak. The peak near $2\theta = 30^{o}$ is composed of an overlap of the broadened (111) and the (004) peaks. Since these reflections are not well resolved, they cannot easily be used to determine lattice parameters, and in particular, cannot be used to track peak shift due to alloying.

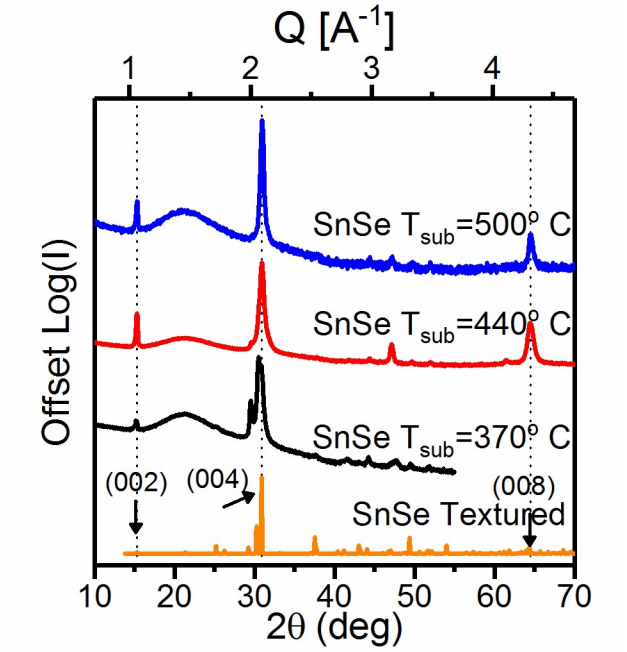

Fig. S2. XRD patterns of SnSe films deposited at different substrate temperatures. The (00l) texture increases with increasing substrate temperature. The reference pattern is for a SnSe film with 40% (00l) texture.

Fig. S3 presents further information about the film texture of the alloy films in the form of 2-dimensional XRD patterns. The angle 2θ is measured radially outward and the angle χ is measured along the azimuthal direction. When interpreting 2D scattering data, it is important to consider the texture or preferential orientation of the crystallographic domains in the sample. Films with isotropic orientation of grains present rings of uniform intensity as a function of χ; these are commonly referred to as powder rings. Textured samples present spots or arcs resulting from scattering from lattice planes with specific orientations with respect to the detector. The OR films are strongly (00ℓ) textured as shown by the spots in Fig. S3a. The RS films have very weak texture and most of them show the characteristic powder rings of Fig. S3b.

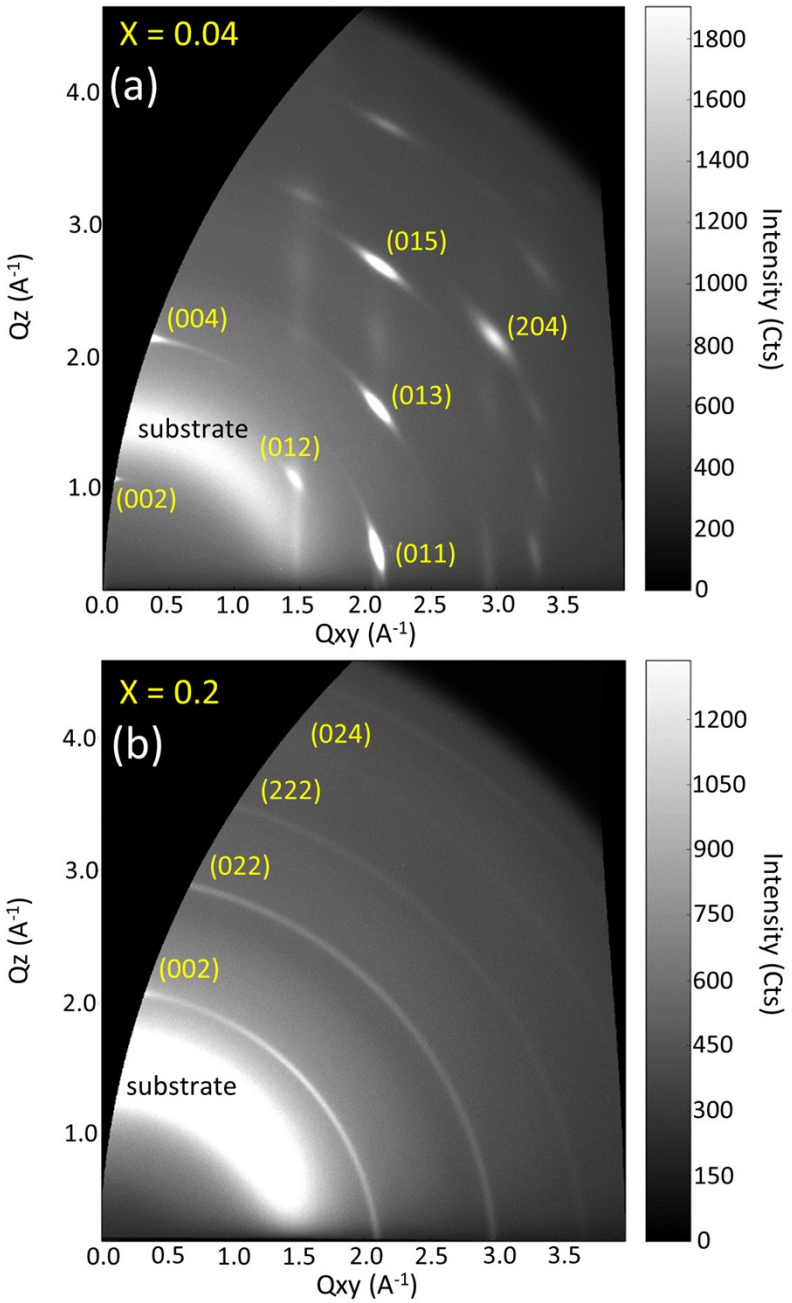

Fig. S3. 2D grazing incidence diffractograms of $Sn_{1-x}Ca_xSe$ films for $x = 0.04$ (OR) and $x = 0.2$ (RS). Only the most intense peaks are marked.

Impurity phases:

$SnSe_2$ is a common competing phase in SnSe growth [1,2]. One signature of $SnSe_2$ is the strong (0001) XRD reflection at $2\theta = 14.4^o$. The OR SnSe (002) reflection appears at $2\theta = 15.3^o$. Fig. S4 shows simulated and experimental XRD patterns of $Sn_{1-x}Ca_xSe$ alloys in the orthorhombic (OR) composition space. These two peaks are quite distinct at $x = 0$, with $\Delta 2\theta \approx 0.9^o$. The shift of the SnSe (002) reflection to smaller 2θ with increasing x in

the simulation (weakly observed in the experiment) does not cause an overlap with the $SnSe_2$ peak position.

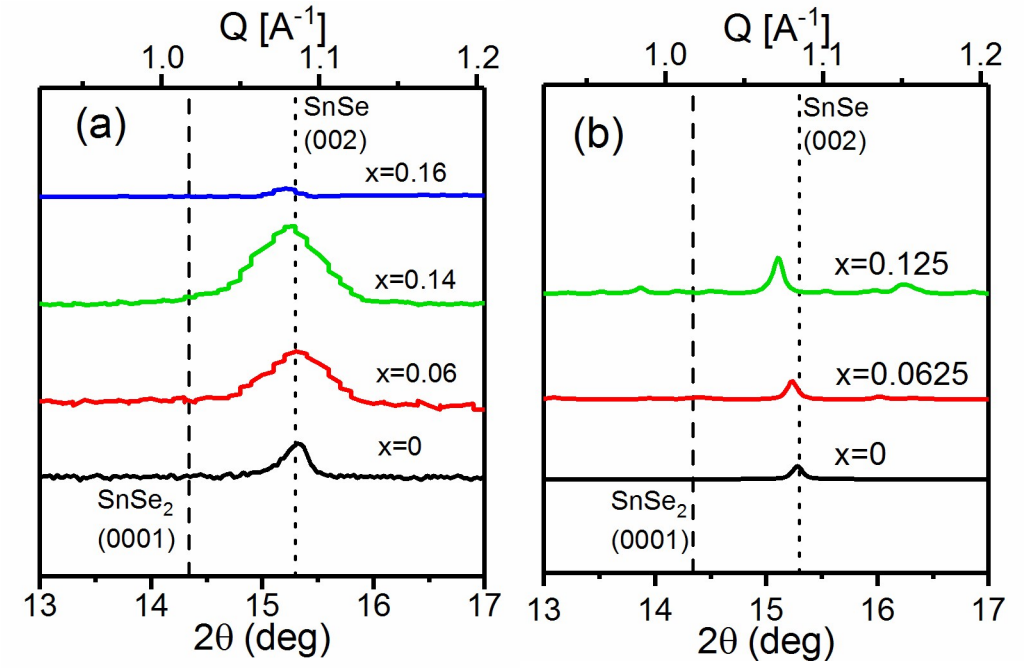

Fig. S4. Experimental (a) and simulated (b) (002) reflections of OR $SnCa_xSe$ alloys ($0 < x < 0.16$) are distinct from the expected $SnSe_2$ (0001) reflection. No $SnSe_2$ is detected in the films.

Electron Diffraction:

The composition analysis and STEM image of the film discussed in Fig. 6 of the main text suggests spinodal decomposition has occurred. We expect the film to exhibit a cubic diffraction pattern and a fluctuating cation composition about an average of $x = 0.2$ in this case. The average composition and fluctuations are as expected, but XRD, which averages over the entire film, indicates that there are both cubic and orthorhombic phases present on the mm-scale, which means that binodal decomposition has occurred in some parts of the film. We therefore perform electron diffraction on the region of the film that exhibits the spinodal decomposition features to determine the structure in that particular region. A nano-probe configuration is chosen over a selected area configuration to gain a narrow beam for diffraction. The nano-probe configuration allows accurate placement of the beam to avoid the substrate and protective layers. Fig. S5 shows the diffraction for the sample shown in Fig. 6 in the text along the cubic [123] axis. Other patterns from several positions on the film along the sample are similarly consistent with the cubic structure. Fits to the orthorhombic structure are consistently poor. We conclude that the electron diffraction images support the interpretation of spinodal decomposition in this sample.

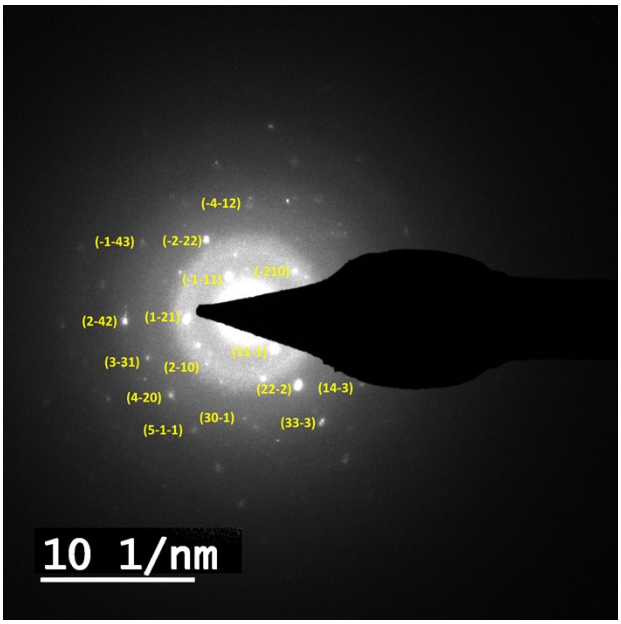

Fig. S5. Nanoprobe electron diffraction pattern of the spinodally-segregated sample shown in Fig. 6 of the main text fitted with cubic indices viewed along the [123] zone axis .

Optical transmission and reflection:

The experimental band gaps in Fig. 7 in the main text are obtained as follows. The transmission T and reflection R of a substrate/film stack are measured by comparing the light transmitted or reflected to the light incident with due regard for any detector dark signal. T and R are shown in Fig. S6a for a $Sn_{0.6}Ca_{0.4}Se$ film. Interference fringes are evident and these are removed by plotting the reflection-corrected transmission $T/(1-R)$, which is interference free, as evident in Fig. S6a. To first order, $T/(1-R) = e^{-\alpha d}$ where α is the absorption coefficient of $Sn_{0.6}Ca_{0.4}Se$ (the substrate is assumed to have no absorption) and d is the film thickness. The energy-dependent absorption coefficients extracted from $T/(1-R)$ are plotted in Fig. 6(b), along with a simulated absorption coefficient based on solutions to the Bethe-Saltpeter equation. A Tauc analysis, a plot of $(\alpha E)^n$ against E with an extrapolation of the linear portion to the axis to obtain E_g (Fig. S6(b)), is used to extract the values reported in Fig. 7 of the main text. For this work, we use $n = ½$ because the band gaps of SnSe and CaSe and most of the intermediate alloy compositions, except near the structural phase transition, are indirect.

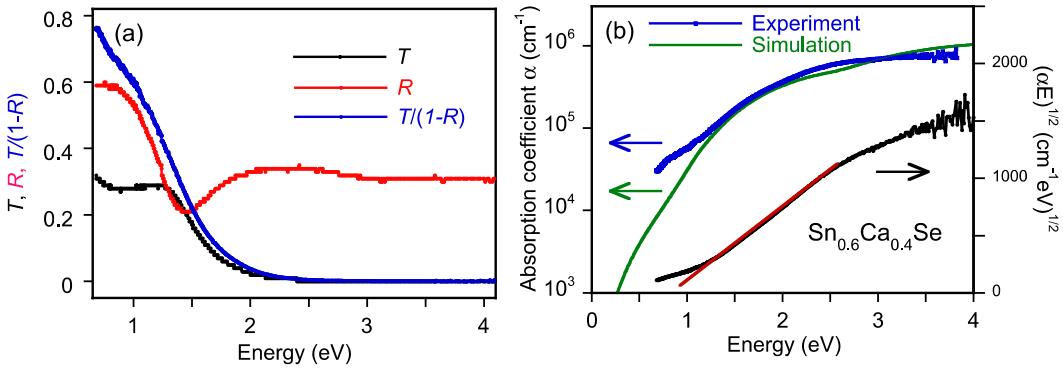

Fig. S6. (a) Transmission *T* (black), reflection *R* (red) and reflection-corrected transmission *T*/(1-*R*) (blue) of a $Sn_{0.6}Ca_{0.4}Se$ film. (b) Absorption coefficient of the same film (blue, left axis) and the simulated absorption (green, left axis). The black data and superimposed red line (right axis) illustrate the $(\alpha E)^{1/2}$ analysis to determine the band gap.

---

1. *Optical and Electrical Properties of $SnSe_2$ and SnSe Thin Films Prepared by Spray Pyrolysis,* D. Martínez-Escobar, M. Ramachandran, A Sánchez-Juárez, J. Sergio Narro Rio. *Thin Sol. Fil.* 585, 390 (2013).
2. *Thermodynamic pathway for the formation of SnSe and $SnSe_2$ polycrystalline thin films by selenization of metal precursors*, P. A. Fernandes, M. G. Sousa, P. M. P. Salomé, J. P. Leitão, A. F. da Cunha, *Cryst. Eng. Comm*. 15, 10278 (2013).